# HYPERSONIC CONTROL FLAP EFFECTIVENESS



D Kumar and J L Stollery
College of Aeronautics, Cranfield University,
Cranfield, Bedford, MK43 0AL, UK

## 1 SUMMARY

The effects of flap deflection, configuration incidence and leading edge bluntness on boundary layer separation and transition have been studied experimentally. A quasi two-dimensional flat plate equipped with a full span trailing edge control flap has been employed for these tests.

The studies have been carried out in a hypersonic gun tunnel at $M_\infty = 8.2$ and $Re_\infty/cm = 9.0 \times 10^4$. The flap deflection angles studied were in the range $0 \leq \delta_f \leq 30°$. The incidence range was from zero to $\alpha = 10°$ (positive $\alpha$ is nose down, see fig. 1). Leading edge bluntness effects were simulated by the introduction of a hemi-cylindrical leading edge.

The flow structure was studied using high speed schlieren photography as well as surface pressure and heat transfer measurements. Liquid crystals were employed to study the three-dimensionality of the flow structure for selected configurations. Analytical theories have been developed to estimate the flap pressure and heat transfer levels for the sharp and blunt configurations. These are compared against experimental measurements.

## 2 SYMBOLS

| | |
|---|---|
| C | Chapman-Rubesin constant |
| $C_D$ | Leading edge drag coefficient |
| $C_H$ | Heat transfer coefficient $q/\rho_\infty U_\infty c_p(T_o-T_w)$ |
| $c_p$ | Specific heat at constant pressure |
| d | Leading edge diameter |
| L | Hingeline length |
| M | Mach number |
| Re | Reynolds number |
| T | Temperature |
| x | distance from the leading edge |
| y | distance normal to surface |
| sublayer | Subsonic portion of boundary layer |
| $\alpha$ | Angle of incidence (°) |
| $\beta$ | Flap deflection (w.r.to flat plate) |
| $\gamma$ | Ratio of specific heats |
| $\theta$ | Shock angle |
| $\delta x$ | change in distance along the plate |
| $\varepsilon$ | $(\gamma-1)/(\gamma+1)$ |
| $\chi$ | Viscous interaction parameter, $M^3\sqrt{(C/Re_x)}$ |
| $\chi_\varepsilon$ | $\varepsilon\,[0.664 + 1.73\,(T_w/T_{o\infty})]\chi$ |
| $\kappa_\varepsilon$ | Bluntness parameter $M^3 C_D \varepsilon\,(d/x)$ |
| $\chi_\varepsilon/\kappa_\varepsilon^{2/3}$ | Bluntness-viscous interaction parameter |

**Subscripts**

| | |
|---|---|
| e | local conditions |
| f | flap |
| i | incipient |
| L | hingeline |
| o | stagnation conditions |
| p | plateau |
| R | reattachment |
| s | shock |
| S | separation |
| w | wall |
| 1 | flat plate conditions |
| 2 | inviscid flap conditions |
| $\infty$ | freestream |

## 3 INTRODUCTION

The aerodynamic requirements of hypersonic flows dictate the intentional blunting of leading edges in order to relieve the local heat transfer and to allow for the installation of active cooling systems. Along with this, the flight envelope of high speed vehicles encompasses a considerable incidence range. These geometry changes influence the aerodynamic properties of the flow over the vehicle and consequently the effectiveness of deflected control surfaces submerged within the body flowfield.

The introduction of bluntness to the leading edge results in a considerable change in the aerodynamic flow structure from that of an equivalent sharp leading edge body. The primary effect is the creation of a bow shock standing off from the leading edge. The increase in the strength of the shock near the leading edge as well as its highly curved structure give rise to gradients in flow properties, such as Mach number and unit Reynolds number along, as well as normal to, the surface of the body.

The shock also creates a region of high temperature, low density flow. These effects are confined to a streamtube whose outer streamlines have been processed by the outer limits of the strong shock and is known as the "entropy layer". As a result of the total pressure losses associated with the strong shock, the local Mach number and unit Reynolds number in this layer are much lower than those in the freestream. In regions dominated by the bluntness effects of the leading edge, the vortical entropy layer envelops the boundary layer

## 4 REVIEW OF LITERATURE

### 4.1 Effect of bluntness on transition

The interaction of the entropy layer with the boundary layer gives rise to a highly complex transition behaviour associated with bluntness. This involves an initial delay of boundary layer transition by the introduction of small leading edge bluntness in comparison with the equivalent sharp body. Further increases in leading edge diameter result in the promotion of transition of the boundary layer.

This behaviour has been studied by Stetson[15] on blunted cones in hypersonic flows. Ericsson[5] has correlated flow transition data on blunted cones for various $Re_d$ at Mach 8. This provides a good illustration of the transition reversal phenomenon. A similar transition reversal behaviour has been observed at supersonic Mach numbers for flat plates by Jillie and Hopkins[7]. Reshotko and Khan[12] have modelled the flow over a blunted flat plate by the method of multiple scales. Stability analysis of the boundary layer flow revealed that the presence of bluntness decreased the critical Reynolds number.

Thus with small bluntness, boundary layer transition occurs further downstream than with the equivalent sharp configuration. For 'large' bluntness, transition occurs upstream of that on the equivalent sharp configuration.

### 4.2 The effect of bluntness on separation

The effects of leading edge bluntness on boundary layer separation were studied using surface pressure measurements by Sanator et al[14]. Their tests revealed that the introduction of leading edge bluntness to 2D-inlet type flows at $M_\infty = 10.55$ and $Re_\infty/cm = 6.1 \times 10^4$ promoted separation. This promotion of separation was attributed to the reduced boundary layer edge Mach number. In the absence of heat transfer measurements, it is not possible to diagnose the state of the boundary layer as either laminar or turbulent although given the freestream conditions, the boundary layer was probably laminar at separation.

The promotion of separation by leading edge bluntness was also observed by Edwards et al[3] in low density tests at $M_\infty = 12.5$ and $Re_\infty/cm = 6.2 \times 10^2$ ($Re_d = 100$). Again the freestream conditions indicate a laminar boundary layer at the hingeline.

Pressure distribution measurements conducted by Vermeulen et al[19] at $M_\infty = 6$ also showed the promotion of separation due to bluntness. Heat transfer tests on corresponding configurations showed that bluntness decreased the heat transfer rate for some distance downstream of the reattachment compression. This was attributed to an increased resistance to transition in the reattachment region due to bluntness. The measurements on the flat plate upstream of the interaction region correlated with heat transfer predictions for laminar boundary layers.

Pressure measurements were conducted by Townsend[18] on a blunted flat plate / flap configuration at $M_\infty = 10.0$ and $Re_\infty/cm = 5.0 \times 10^4$ ($Re_d = 25000$). The measurements were limited to locations ahead of the hingeline and showed that there was an appreciable reduction in the extent of the separated flow region when leading edge bluntness was introduced. The state of the boundary layer was not diagnosed although it was suspected to be laminar upstream of the interaction region.

In tests at $M_\infty = 10.0$ and $Re_\infty/cm = 8.4 \times 10^4$ on a compression corner, Coet et al[20] found that the introduction of hemi-cylindrical bluntness at the leading edge delayed separation of laminar boundary layers for $21000 \le Re_d \le 41000$. These tests also showed an order of magnitude decrease in heat transfer on the flap when the leading edge diameter was increased from 0 mm to 2.5 mm. This was attributed by the authors to losses in stagnation pressure sustained at the leading edge. Further increasing the leading edge diameter to d = 5 mm reduced the length of separated flow region but increased the flap heat transfer level. This latter effect may be due to the promotion of transition in the flap boundary layer.

Measurements on blunt compression corners by Holden[9] at $M_\infty = 19$ and $\beta = 25.7°$ showed that the extent of the laminar separated region was related to the viscous bluntness interaction parameter, $\chi_\varepsilon/\kappa_\varepsilon^{2/3}$. This effectively accounted for the relative effects of changes in Mach number and Reynolds number on the extent of the interaction.

Holden's results indicate that for $\chi_\varepsilon/\kappa_\varepsilon^{2/3} \le 0.1$, the introduction of leading edge bluntness results in a dramatic reduction in the extent of boundary layer separation while for $0.1 \le \chi_\varepsilon/\kappa_\varepsilon^{2/3} \le 0.5$, leading edge bluntness promotes separation. Due to the relatively high Mach number and the low freestream unit Reynolds number, it is believed that these tests were entirely laminar.

Thus, 'small' bluntness promotes separation with respect to equivalent sharp configuration while 'large' bluntness delays it.

## 5 ANALYTICAL MODELS

### 5.1 Reference temperature theory

Using the concepts of similarity, flat plate equivalence and a reference temperature, Stollery and Coleman[16] demonstrated the dependence of heat transfer on the local pressure for turbulent boundary layers in regions of strong pressure gradients. Based on similar concepts, Vermeulen et al[19] suggest a more universal expression for the heat transfer distribution for laminar and turbulent boundary layers as

$$C_H Re_{\infty x}{}^n = \frac{A}{s}\left[\frac{U_e \rho_e}{U_\infty \rho_\infty}\right]^{(1-n)}\left[\frac{T_\infty}{T^*}\right]^{(1-2n)} C^{*n}\left[\frac{T_r - T_w}{T_o - T_w}\right] \qquad (1)$$

where the constants A = 0.332, $s = Pr^{2/3}$ and n = 0.5 for laminar boundary layers and A = 0.0296, s = 1 and n = 0.2 for turbulent boundary layers.The effects of compressibility on the flat plate heat transfer rate are accounted for by using Eckert's reference enthalpy method. Hence, both authors use the expression

$$T^* = T_e + 0.5(T_w - T_e) + 0.22r\left(\frac{\gamma-1}{2}\right)M_e{}^2 T_e \qquad (2)$$

In the theoretical predictions, the recovery factor used for calculating the reference temperature for both laminar and turbulent boundary layers has been taken as $Pr^{1/2}$.

### 5.2 Virtual origin for theoretical calculations

For attached turbulent flows, Stollery et al[16] found that the method with the origin of the solution located at the leading edge successfully predicted the skin friction and heat transfer through the interaction region.

For separated flows, Vermeulen et al[19] used the peak heat transfer location as a virtual origin together with the inviscid flap pressure to predict the flap heat transfer. This gave good agreement with the measured flap heat transfer for locally laminar or turbulent flows. However, in both cases, the solution failed to predict the heat transfer distribution in the separation region.

In the present calculations, the leading edge has been assumed as the origin for attached laminar and turbulent flows. For separated laminar flows, the flap estimates have used the leading edge as the virtual origin whilst for separated turbulent flows the hingeline has been used as the virtual origin. For both attached and separated flows, the measured pressure distributions have been used in the calculations of the flap heat transfer.

### 5.3.1 Sharp leading edge ($\alpha = 0°$)

The local flap Mach number, temperature and flow velocity have been estimated from wedge tables[1] assuming inviscid flow over the flat plate. This neglects any stagnation pressure losses sustained at the leading edge shock. At an incidence $\alpha = 0°$, this shock is caused by viscous interaction at the leading edge.

The estimated local Mach number together with the other parameters has been used to estimate the flap reference temperature from eq.(2). The combination of these parameters with the measured pressure levels has been used to estimate the flap heat transfer levels from eq. (1).

### 5.3.2 Sharp leading edge ($\alpha > 0°$)

The local flat plate conditions have been calculated from the wedge tables. The hingeline Mach number together with the flap deflection angle has been used to determine the local flow parameters on the flap. These parameters have been employed with the measured pressure distributions to predict the flap heat transfer variation.

### 5.3.3 Blunt leading edge ($\alpha = 0°$)

The processing of the surface and near surface streamtubes by a strong, near-normal shock results in a considerable loss of stagnation pressure. The strong shock also produces an increase in pressure at the leading edge. At zero incidence, this subsequently decreases along the flat plate to the freestream pressure level. The present authors[21] have shown that the experimental distribution can be modelled using blast wave theory. The best approximation was found using the second order theory proposed by Lukasiewicz[10]. This gives the pressure as

$$\frac{p}{p_\infty} = 0.127 M_\infty^2 \left[\frac{C_D}{x/d}\right]^{2/3} + 0.56 \qquad (3)$$

By assuming isentropic flow following the stagnation pressure loss at the leading edge and the above pressure variation, the inviscid Mach number, temperature and flow velocity at the hingeline have been estimated.

The conditions at the beginning of the flap (downstream of the flap shock, point 2 in figure 2(b)) have been estimated using the hingeline conditions as the effective supersonic freestream, a method proposed by Richards[13] for strong bluntness. The stagnation pressure along the surface streamtube on the flap has been assumed as constant and equal to its value at the beginning of the flap.

The local Mach number, flow velocity and temperature at a given point on the flap have been calculated from the flap surface streamtube stagnation pressure combined with the measured static pressure. These have subsequently been used to estimate the flap heat transfer rate using reference temperature theory as outlined in section 5.1.

### 5.4 The effect of Mach shear in the entropy layer

The flow properties on streamlines at the hingeline (upstream of the flap shock, point 1 in figure 2(b)) depend on the local static and stagnation pressures. For the inviscid flow, it has been assumed that the pressure gradient normal to the streamlines is zero. This is reasonable if the streamline curvature at the hingeline is negligible.

As a result of the highly curved leading edge shock, a normal gradient in stagnation pressure is produced. The shock shape is given by blast wave theory (Anderson[2]) as

$$\frac{Y_s}{d} = 0.774 C_D^{1/3} \left(\frac{x}{d}\right)^{2/3} \qquad (4)$$

By differentiating the shock angle may be calculated from

$$\left[\tan\theta_s\right]_{y=Y_s} = \left[\frac{dY_s}{dx}\right]_{y=Y_s} = 0.516 C_D^{1/3} \left(\frac{x}{d}\right)^{-1/3} \qquad (5)$$

Assuming that the streamline deflection through this shock to be negligible, the downstream stagnation pressure on a streamline at y = Ys can be calculated. This model is shown in figure 2(a). Together with the assumption that the conditions along a streamline downstream of the leading edge shock are isentropic and the hingeline static pressure is equal to the blast wave pressure, the inviscid Mach number profile at the hingeline can be estimated.

The incident hingeline Mach profile was combined with Elfstrom's[4] shear interaction model, shown in figure 2(b) to estimate the effects of the Mach number gradients on the flap pressure distribution.

The flap shock was faceted. The local facet angle at $y = Y_s$ was determined from the upstream Mach number and a requirement to deflect the streamline parallel to the flap surface. The pressure immediately downstream of the facet was convected to the surface along a Mach line. The Mach angle was determined by the Mach number immediately downstream of the shock facet.

The Mach shear at the hingeline has also been estimated from the entropy layer pitot pressure measurements of Stone[17] at Mach 10.4. This was chosen to represent the hingeline Mach number profile in the present test due to its similar value of $C_D/(x/d)$. The local Mach number was inferred from Stone's measurements using the Rayleigh-pitot formula given by the Ames tables[1].

Near the surface, the predicted Mach number profile was in good agreement with the profile given by Stone's[17] measurements. Further away from the surface, the predicted Mach number exceeded the measured value by 40%.

## 6 WIND TUNNEL FACILITY

The Cranfield hypersonic gun tunnel facility was used for the investigations. The tests were carried out with air as the working gas. An axisymmetric contoured nozzle provided a useful test jet diameter of 15.0 cm at a freestream Mach number of 8.2. The tunnel is equipped with a single pass schlieren system. This uses a high intensity microsecond duration argon spark source to illuminate density gradients in the flow. Pressure measurements were carried out using Kulite XCS-190 series pressure transducers. Heat transfer measurements were made using surface mounted thin film platinum gauges on a Macor substrate. The temperature history of the gauges was integrated using a low noise, high bandwidth analogue integrator circuit. The models used for the present tests are shown in figure 1.

## 7 RESULTS AND DISCUSSION

### 7.1 The effect of flap deflection (sharp LE)

#### 7.1.1 Attached flows ($\alpha = 0°$)

A flap deflection of $\beta = 5°$ creates an oblique shock near the hingeline. The single flap shock implies that the flow is attached through the interaction. The flap boundary layer appears laminar.

The compression associated with the shockwave produces an increase in pressure on the flap, as can be seen in figure 3(a). The increase starts upstream of the hingeline due to a deflection of the inviscid flow by the thickening of the subsonic portion of the boundary layer. The theoretical pressure ratio of 2.5 from wedge theory agrees well with the measured ratio of 2.7.

The compression which results from the shockwave causes a decrease in the total thickness of the boundary layer on the flap. This is due to an increase in density and velocity in streamtubes in the supersonic portion of the boundary layer.

For the configuration $\alpha = 0°$, $\beta = 5°$, the predictions of reference temperature theory for the flap heat transfer distribution assuming a fully laminar or a fully turbulent flap boundary layer are shown in figure 5(i). The method outlined in section 5.3.1 has been used for these predictions.

The agreement between the experimental heat transfer measurements and the predictions of the laminar theory reinforce the schlieren observation that the flap boundary layer is laminar. For attached laminar flows, the increase in heat transfer on the flap downstream of the interaction region is a direct function of the pressure increase across the flap shock.

#### 7.1.2 Separated flows ($\alpha = 0°$)

An increase in flap deflection increases the strength of the flap shockwave. This is accompanied by an increase in the local adverse pressure gradient. At a certain flap deflection, the adverse pressure gradient reduces the wall skin friction to zero at the hingeline. This flap deflection is known as the incipient separation condition.

Deflection of the flap beyond this angle produces a separated flow with separation and a reattachment points upstream and downstream of the hingeline respectively. Both of these points are characterised by local shockwaves. The dual shock interaction structure differentiates separated flows from the single shock structure of attached flows.

The Needham & Stollery[11] incipient separation criterion gives the incipient separation flap angle as

$$M_\infty \beta_i = 80 \bar{\chi}_L^{\,1/2} \qquad (6)$$

This result was verified theoretically by Inger[6] using triple-deck theory. Under the present test conditions, the flap deflection for incipient separation is 6.6°. In figure 3, whilst for $\beta = 5°$, the flow is attached, the dual shock structure for $\beta = 10°$ indicates that the flow has separated. This supports the prediction of the above criterion.

Further increasing the flap deflection angle results in an upstream movement of the separation point and for well-separated flows, a pressure plateau develops. In accordance with the concept of free-interaction, the plateau pressure level attained correlates well with the correlation given by Needham[11], as shown in figure 4(a). This gives the plateau pressure as

$$\frac{p_P}{p_\infty} = 1 + 1.2 \bar{\chi}_s^{\,1/2} \qquad (7)$$

The impingement of the shear layer on the flap and the subsequent formation of a reattachment shock causes the pressure to increase on the flap. This pressure rise increases with the deflection angle and causes a significant thinning of the flap boundary layer as seen from the schlieren photographs of figure 2.

The subsequent increase in heat transfer in the interaction region suggests that the shear layer has become transitional. This is also suggested by the schlieren photograph of the $\beta = 25°$ configuration shown in figure

3(e) which shows the presence of shockwaves at the edge of the shear layer.

It has been assumed that the shear layer becomes transitional at the first departure from the minima in heat transfer following separation. This is shown in figure 4(b).

Although the transition of the shear layer causes only a moderate increase in heat transfer upstream of the hingeline, its effects on the heat transfer levels on the flap are dramatic as shown in figure 5.

For $\beta$ = 5°, the increase in heat transfer on the flap is a direct consequence of the increased local compression. The absence of separation means that shear layer instability is avoided and the flap boundary layer remains laminar.

For $\beta$ = 15°, the length of separated flow and the subsequent promotion of transition in the unstable shear layer results in flap heat transfer levels which are significantly above the predicted laminar level along the entire length of the flap. By the trailing edge of the flap, the process of transition is complete and the local turbulent heat transfer level is attained. In this case, the heat transfer level on the flap increases due to the both promotion of transition by the shear layer and the local compression process.

For $\beta$ = 25°, the increase in the length of the shear layer promotes transition from upstream of the hingeline and the process of transition is completed within the separation region. As a result, the heat transfer levels realised on the flap correlate well with the predictions for a fully turbulent flap boundary layer along the entire length of the flap.

#### 7.1.3 Similarity between incipient and well-separated flows ($\alpha = 0°$)

Using an order of magnitude analysis, Needham[11] showed that the hypersonic similarity parameter for incipient separation $M_{\infty}\alpha_i$ is a function of the local viscous interaction parameter. A similar argument may be applied to the separation streamline to show the dependence of the separation angle on the local viscous interaction parameter.

The similarity is shown in figure 6(a) for laminar interactions. The angle of the separation streamline has been calculated geometrically using the measured locations of separation and reattachment. For laminar flows, the separation data correlates as

$$M_{\infty}\beta_{sep} = 50\left[\bar{\chi}_{sep}\right]^{1/2} \tag{8}$$

Theoretical analysis using triple deck theory by Inger[6] has shown that the separation streamline obeys the same scaling laws as the incipient separation flap deflection angle.

### 7.2 The effect of incidence (sharp leading edge)

#### 7.2.1 Flat plate flows ($\alpha \geq 0°$)

At zero incidence, the leading edge shock is present due to the finite displacement thickness of the boundary layer. The introduction of incidence and the associated increase in the required streamline deflection angle increases the strength of the leading edge shock.

The increase in the shock strength with incidence decreases the local Mach and increases the local unit Reynolds numbers at the edge of the boundary layer. The ratio of the local to freestream unit Reynolds number can be written as

$$\frac{Re_e}{Re_{\infty}} = \frac{\rho_e}{\rho_{\infty}} \cdot \frac{U_e}{U_{\infty}} \cdot \frac{\mu_{\infty}}{\mu_e} \tag{9}$$

A linear viscosity-temperature relationship was used together with the expressions given by the Ames tables to estimate the local to freestream unit Reynolds number ratio. The effect of incidence on the local Mach number and unit Reynolds number under the freestream conditions of the present study is shown in figure 7.

The flat plate heat transfer distributions shown in figure 8 show that the boundary layer is laminar for $\alpha$ = 0° along the entire flat plate. At $\alpha$ = 5° the boundary layer is laminar up to the hingeline. There is a deviation from the laminar heat transfer level at x/L = 1.05. This is due to the onset of boundary layer transition. At $\alpha$ = 10°, the onset of transition occurs at about x/L = 0.6 i.e. well ahead of the hingeline.

The decrease in the local flat plate Mach number with incidence decreases the transition Reynolds number. The increase in the local unit Reynolds number means that the transition Reynolds number is attained over a shorter length. Thus the changes in both of these parameters with incidence promotes transition of the flat plate boundary layer.

#### 7.2.2 Attached flows ($\alpha \geq 0°$)

For incidences of 0°, 5° and 10° with $\beta$ = 5°, there is no sign of separation. There is a single oblique shock at the hingeline indicating an attached flow structure. This is confirmed by the absence of a hingeline pressure plateau in the corresponding pressure distributions, shown in figure 10.

The pressure distributions also show that the start of the interaction moves downstream as the incidence increases from $\alpha$ = 0° to $\alpha$ = 5°. The heat transfer distributions for both of these configurations decreases near the hingeline. This is typical of a laminar interaction and confirms that the equivalent flat plate boundary layer is laminar at the hingeline for both configurations.

The start of the interaction is further delayed at an incidence $\alpha$ = 10°. For this configuration, there is no discernible increase in pressure upstream of the hingeline.

The local decrease in heat transfer in this region is also much smaller than for the other two configurations.

For $\alpha = 10°$, the transition of the flat plate boundary layer upstream of the hingeline energises the subsonic portion of the boundary layer. This offsets the local momentum decrease associated with the flap adverse pressure gradient and thus reduces the thickening of the sublayer. This in turn reduces the pressure rise in the upstream interaction region. The increased resistance to the adverse pressure gradient due to transition ahead of the hingeline also means that the loss of heat transfer upstream of the hingeline is absent.

### 7.2.3 Separated flows ($\alpha \geq 0°$)

The effects of incidence for $\beta = 10°$ are shown in figure 11. This shows a delay in separation as the incidence is increased to $\alpha = 5°$. This is confirmed by the pressure and heat transfer distributions shown in figure 12(a) and (b). The flat plate heat transfer distributions at this incidence, shown in figure 9(b), shows that the boundary layer is laminar upstream of the hingeline.

According to the incipient separation criterion given by eq. 6, a decrease in the local Mach number and an increase in the local Reynolds number both promote separation. The inviscid calculations of local Mach and Reynolds numbers of figure 7 shows that the Mach number decreases and the local Reynolds number increases as the incidence of the flat plate is increased. This should result in an increase the length of the separated flow. The observations of the present tests at $\alpha = 5°$ are contrary to the predictions.

Using an analysis similar to that used by Stollery et al[16], the skin-friction distribution on a flat plate at incidence with a laminar boundary layer (assuming $u_e = u_\infty$) is given by

$$c_{f\infty} = \frac{0.664}{Re_{\infty x}^{0.5}}\left(\frac{p_e}{p_\infty}\right)^{0.5} \qquad (10)$$

This when coupled with Needham's[11] order of magnitude analysis of incipient separation gives the incipient separation flap angle at incidence as

$$M_\infty \beta_i = 80\bar{\chi}_{\infty_L}{}^{1/2}\left[\frac{M_e}{M_\infty}\left(\frac{p_e}{p_\infty}\right)^{1/2}\right]^{1/2} \qquad (11)$$

For $\alpha = 5°$, the incipient separation flap angle assuming the flow to be laminar is 7.8°. The delay in separation at incidence arises due to the increase in the flat plate pressure level.

For $\alpha = 10°$, eq. 12 predicts $\beta_i = 8.4°$ for laminar interaction. The schlieren photograph of figure 11 suggests that the flow is attached for $\alpha = 10°$, $\beta = 10°$. This is confirmed by the absence of a plateau in the pressure distribution of figure 12. The increase in the experimental incipient separation angle above the value predicted by eq. 12 is due to the transition of the boundary layer upstream of the hingeline.

## 7.3 The effects of bluntness ($\alpha = 0°$)

Blunting the leading edge of a flat plate increases both the pressure and the heat transfer distributions along the length of the flat plate as shown in figure 13. The increases are due to the presence of a strong detached bow shockwave. The stagnation pressure loss sustained at the leading edge decreases the boundary layer edge Mach number at the hingeline. An increase in the leading edge diameter increases the thickness of the entropy layer. This causes a reduction in the local Mach number at a given height above the surface

### 7.3.1 Attached flow ($\alpha = 0°$)

For $\alpha = 0°$, $\beta = 5°$, flow visualisation of the blunted configurations shown in figure 14 shows a single shock. Thus with this flap angle, the flow remains attached for all levels of bluntness. The reduction in hingeline Mach number increases the angle of the flap shock. The density gradients associated with the entropy layer mask the gradients associated with the boundary layer. This makes the identification of transition in the boundary layer very difficult for blunted configurations.

For $\alpha = 0°$, $\beta = 5°$, the pressure and heat transfer distributions are shown in figure 15(a). The reduced hingeline Mach number decreases the pressure recovered on the flap with the blunt leading edge. The decrease in heat transfer in the upstream interaction region for both the sharp and the blunt configurations as shown in figure 17(a) means that the hingeline boundary layers for both configurations are laminar at the start of the interaction.

For $\beta = 5°$, the laminar and turbulent flap heat transfer levels for the sharp and blunt leading edge configurations has been estimated using the reference temperature theory given in section 5.3.1 and 5.3.3 respectively. These are compared against the distributions for the equivalent sharp leading edge configuration in figure 17(b). The agreement with laminar predictions suggests that the flap boundary layer in both cases is laminar.

### 7.3.2 Separated flow ($\alpha = 0°$)

Schlieren flow visualisation of the $\beta = 10°$ configuration with a progressive increase in the leading edge diameter is shown in figure 16. The introduction of bluntness delays separation of the boundary layer. The dual shock interaction structure of the sharp leading edge configuration means that this flow is well separated whilst for d = 4 and 6.0 mm, the single flap shock implies that the suppression of separation is complete and the flow is attached.

This is confirmed by pressure and heat transfer measurements for the sharp and the blunt (d = 6 mm) configurations, shown in figure 17(a). The sharp configuration displays the characteristic plateau pressure between separation and reattachment indicative of a well-separated flow. The equivalent blunt configuration pressure distribution is typical of an attached flow with the increase occurring from the immediate vacinity of the hingeline.

The sharp and blunt leading edge flap heat transfer distributions for $\beta = 10°$ are compared against theory in figure 17(b). Since the measurements for both of these configurations are between their respective laminar and turbulent levels, they are both probably transitional.

The transition of the flap boundary layer for the sharp configuration of $\alpha = 0°$, $\beta = 10°$ is promoted by the formation of a separated shear layer and an adverse pressure gradient. The absence of a separation and the lower adverse pressure gradient for the equivalent blunt configuration would lead to the initial conclusion that transition of the flap boundary layer should be delayed.

Surface flow visualisation using liquid crystal techniques displayed a number of periodic spanwise peaks and troughs in temperature on the blunt configuration. These originated at the leading edge of the body and are due to the formation of streamwise Taylor-Gortler vortices. For blunted leading edges, concavity occurs as streamlines negotiate the curvature ahead of the leading edge between the bow shock and the body.

For well-separated flows, ($\beta = 25°$) the progressive delaying of separation by bluntness is shown in figure 18. Comparison of the pressure and heat transfer distributions for well-separated blunted flows is shown in figure 19. Comparison of these measurements with their equivalent sharp configurations in figure 4 shows that bluntness reduces the flap pressure and heat transfer levels.

Although the leading edge stagnation pressure losses considerably reduce the flap heat transfer level, transition of the boundary layer is again promoted by flap deflection. This is evident from the agreement between the measured and calculated turbulent heat transfer levels, as shown in figure 20. The flap boundary layer changes from laminar for $\beta = 5°$ to transitional at $\beta = 15°$ and to a turbulent structure at $\beta = 25°$.

### 7.3.3 Mach shear interaction effect ($\alpha = 0°$)

For the blunted configuration with $\alpha = 0°$, $\beta = 25°$, the reattachment pressure rise on the flap is followed by a secondary compression, as shown by figure 19. This secondary rise is associated with the interaction of the flap shock with the Mach number gradient associated with the entropy layer.

An estimate of this effect has been made using the models proposed in section 5.4. The results are shown in figure 21(a). The predictions using a hingeline Mach number profile inferred from the leading edge shock shape significantly overestimate the interaction pressure. The experimentally derived Mach number profile from Stone's[17] pitot pressure data provides good agreement with the experimental measurements of the flap shear interaction effects. The difference in accuracy towards the trailing edge of the flap arises due to the overestimation of Mach numbers in the entropy layer in the theoretically predicted profile.

For flap angles in the range $5° \leq \beta \leq 30°$, the measured flap pressure levels at the front ($x/L = 1.069$) and the back end of the flap ($x/L = 1.226$) are plotted in figure 21(b). For small flap deflections, since the penetration of the flap into the entropy layer is small, the difference in pressure between the beginning and the end of the flap is small. As the flap deflection angle is increased, the penetration of the flap into the entropy layer increases and leads to an measurable increase in pressure between the beginning and the end of the flap.

The leading edge shock derived Mach number profile and the experimentally derived Mach number profile provide good agreement with the measurements at the front of the profile. This is because the pressure at the front of the flap is determined primarily by the surface Mach number.

At the end of the flap, the measurements are in agreement with the predictions made using the Mach number profile derived from Stone's[17] data. However, at the end of the flap, the leading edge shock derived Mach profile model produces a considerable overestimation at high flap deflections. This is due to the overestimation of Mach number away from the surface by this model.

## 8 CONCLUSIONS

Flap deflection promotes separation of laminar boundary layers. It also promotes the transition of the boundary layer

Incidence promotes transition of the flap boundary layer. It delays separation for both laminar and transitional boundary layers.

The introduction of large bluntness, under the present conditions, substantially delays separation of the boundary layer upstream of a compression corner.

Bluntness also reduces the pressure recovered downstream of the hingeline and hence causes significant loss of control effectiveness.

Transition of the flap boundary layer is promoted by large bluntness. Bluntness alleviates flap heat transfer for both laminar and turbulent flap boundary layers.

## 9 ACKNOWLEDGEMENTS

The work presented in this paper was conducted as part of a Total Technology PhD programme. It was sponsored by Science and Engineering Research Council with British Aerospace, Stevenage as the industrial sponsor.

## 10 REFERENCES

1) *Ames Research Staff (1953)* : Equations, tables and charts for compressible flows NACA-R-1135

2) *Anderson J D Jr (1989)* : Hypersonic and high temperature gas dynamics, McGraw Hill

3) *Edwards C L W, Anders J B (1968)* : Low density, leading edge bluntness and ablation effects on wedge induced laminar

boundary layer separation at moderate enthalpies in hypersonic flows NASA TN D-4829
4) *Elfstrom, G M (1972)* : Turbulent hypersonic flow at a wedge-compression corner J. Fluid Mech., vol. 53, part 1, pp 113-127
5) *Ericsson L E (1988)* : Effects of nose bluntness and cone angle on slender vehicle transition AIAA J. vol. 26, no. 10 Oct. 1988
6) *Inger G R (1993)* : Scaling of incipient separation in high speed laminar flows, AIAA-93-3435
7) *Jillie D W, Hopkins, E J (1961)* : Effect of Mach number, leading edge bluntness and sweep on boundary layer transition on a flat plate NASA TN-D 1071 (1961)
8) *Hayes W D, Probstein R F (1966)* : Hypersonic flow theory volume 1 - inviscid flows, Academic Press
9) *Holden M (1975)* : Experimental studies in shockwave-boundary layer interactions AGARD AG-203
10) *Lukasiewicz J (1961)* : Hypersonic flow blast analogy AEDC TN-61-158
11) *Needham D A (1965)* : Laminar separation in hypersonic flows PhD thesis, University of London,
See also *Needham & Stollery* AIAA Paper 66-455 (1966)
12) *Reshotko E, Khan M M S (1979)* : Stability of a laminar boundary layer on a blunted flat plate in supersonic flow - Laminar-Turbulent transition, IUTAM Symposium, Stuttgart September 1979, pp 189-200
13) *Richards G (1978)* : High speed flow over two-dimensional and axi-symmetric bodies, PhD Thesis, Cranfield Institute of Technology
14) *Sanator R J, Boccio J L, Shamshins D (1968)* : Effects of bluntness on hypersonic two-dimensional inlet type flows NASA CR-1145
15) *Stetson K F (1983)* : Nose bluntness effects on cone frustum boundary layer transition in hypersonic flow AIAA 83-1763
16) *Stollery J L, Coleman, G T (1975)* : A correlation between pressure and heat transfer distributions at supersonic and hypersonic speeds (Aeronautical Quarterly, Nov., pp 304 - 312)
17) *Stone, H W (1969)* : The leading edge effects on the laminar flat plate boundary layer and the aerodynamic heating at Mach 10.4, NASA TN-D 5160
18) *Townsend J C (1966)* : Effects of leading edge bluntness and ramp deflection angle on laminar boundary layer separation in hypersonic flow, NASA TN-D 3290
19) *Vermeulen J P, Simeonides, G (1992)* : Parametric study of shockwave / boundary layer interactions over 2-D compression corners at Mach 6,VKI TN-181
20) *Coet M C, Delery J, Chantez B (1992)* : Experiments on shockwave - boundary layer interaction at high Mach number with entropy layer effect, IUTAM Symposium, Marseille
21) *Kumar D, Stollery J L (1993)* : The effect of leading edge bluntness on control effectiveness at hypersonic speeds, 19th International Symposium on Shock Waves, July 1993, Marseille

## 11 FIGURES

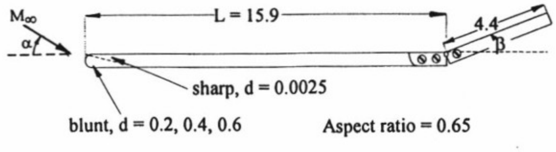


All tests conducted at $M_\infty = 8.2$, $Re_\infty/cm = 9.0 \times 10^4$

**FIG. 1 GEOMETRIES OF THE CONFIGURATIONS USED FOR THE PRESENT TESTS (all dimensions in cm)**

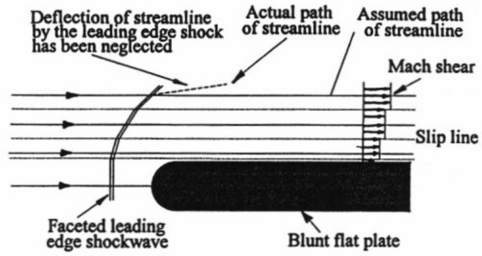


**(a) leading edge shock based model employed to estimate entropy layer Mach no. profile over the blunt flat plate**

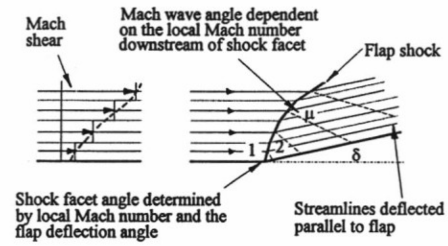


**(b) model used to calculate the effects of entropy layer Mach shear on flap pressure distribution**

**FIG. 2 MODELS EMPLOYED TO ESTIMATE THE FLAT PLATE AND FLAP FLOW PROPERTIES ALONG STREAMLINES IN THE ENTROPY LAYER**

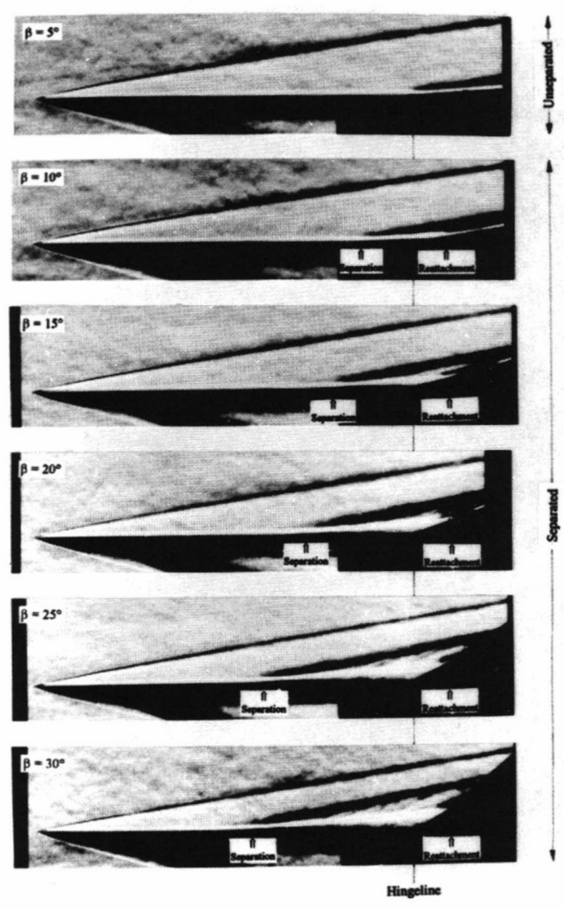


FIG. 3 THE EFFECT OF FLAP DEFLECTION ON SEPARATION [$M_\infty = 8.2$, $Re_\infty/cm = 9.0 \times 10^4$, $\alpha = 0°$, Sharp leading edge]

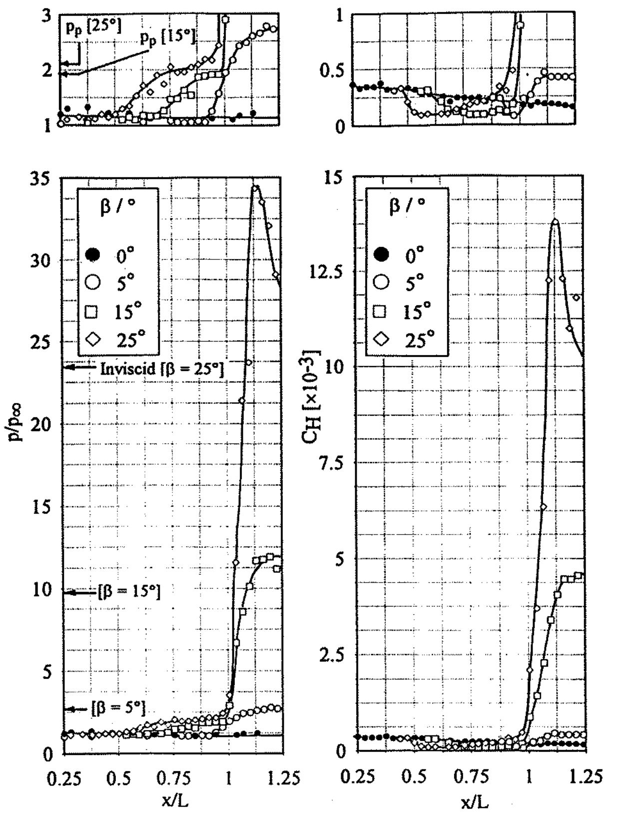


(i) pressure (ii) heat transfer

FIG. 4 THE EFFECT OF FLAP DEFLECTION ON THE PRESSURE AND HEAT TRANSFER DISTRIBUTIONS IN THE INTERACTION REGION [$M_\infty = 8.2$, $Re_\infty$/cm = 9.0 ×10$^4$, $\alpha$ = 0°, sharp leading edge]

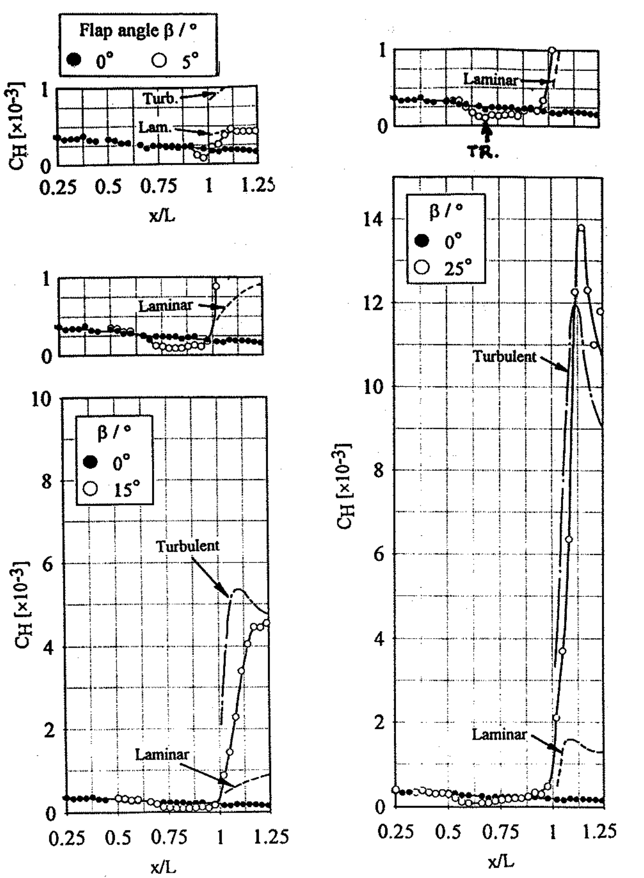


FIG. 5 COMPARISON OF THE FLAP HEAT TRANSFER DISTRIBUTIONS WITH PREDICTIONS FOR LAMINAR AND TURBULENT BOUNDARY LAYERS [$M_\infty = 8.2$, $Re_\infty$/cm = 9.0 ×10$^4$, $\alpha$ = 0°, sharp leading edge]

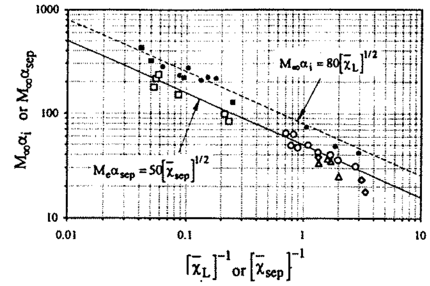


FIG. 6 CORRELATION BETWEEN INCIPIENT SEPARATION FLAP ANGLE AND WELL-SEPARATED FLOW STREAMLINE DEFLECTION ANGLE

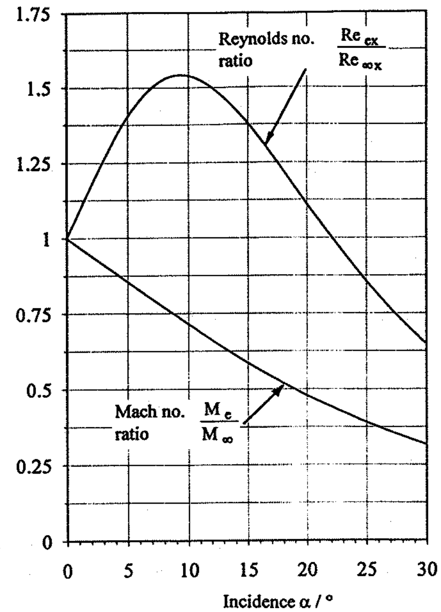


FIG. 7 THE EFFECT OF INCIDENCE ON THE INVISCID CONDITIONS OVER THE FLAT PLATE [$M_\infty = 8.2$]

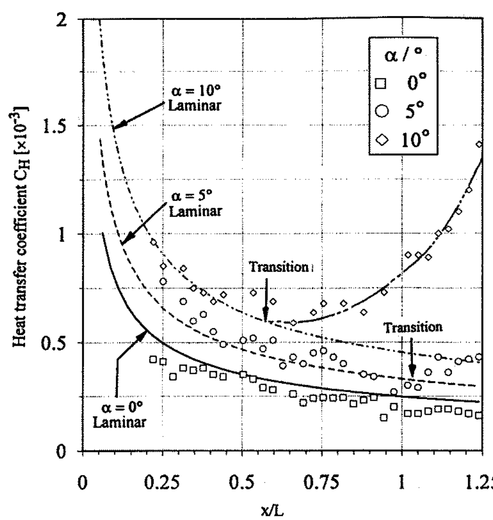


FIG. 8 THE EFFECT OF INCIDENCE ON FLAT PLATE HEAT TRANSFER DISTRIBUTION [$M_\infty = 8.2$, $Re_\infty$/cm = 9.0 ×10$^4$, sharp leading edge]

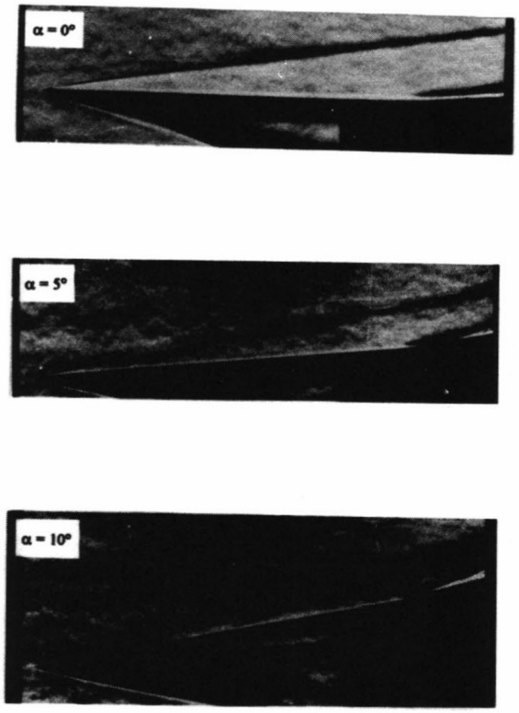


FIG. 9 THE EFFECT OF INCIDENCE ON ATTACHED FLOWS
[$M_\infty = 8.2$, $Re_\infty/cm = 9.0 \times 10^4$, $\beta = 5°$, Sharp leading edge]

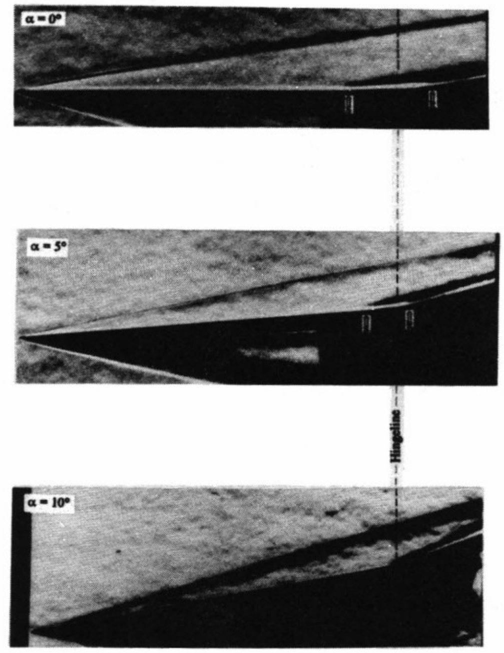


NOTE : S = Separation point, R = Reattachment point

FIG. 11 THE EFFECT OF INCIDENCE ON SEPARATED FLOWS
[$M_\infty = 8.2$, $Re_\infty/cm = 9.0 \times 10^4$, $\beta = 10°$, Sharp leading edge]

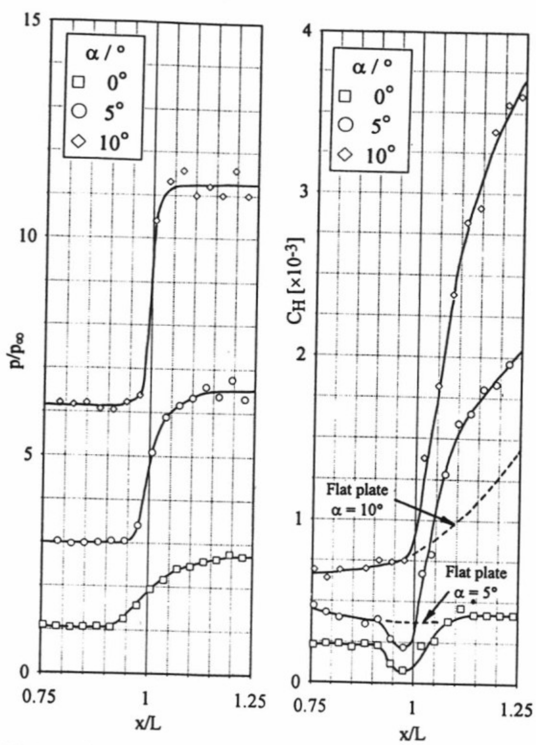


FIG. 10 THE EFFECT OF INCIDENCE ON THE PRESSURE AND HEAT TRANSFER DISTRIBUTIONS IN THE FLAP INTERACTION REGION FOR ATTACHED FLOWS [$M_\infty = 8.2$, $Re_\infty/cm = 9.0 \times 10^4$, $\beta = 5°$, sharp leading edge]

5

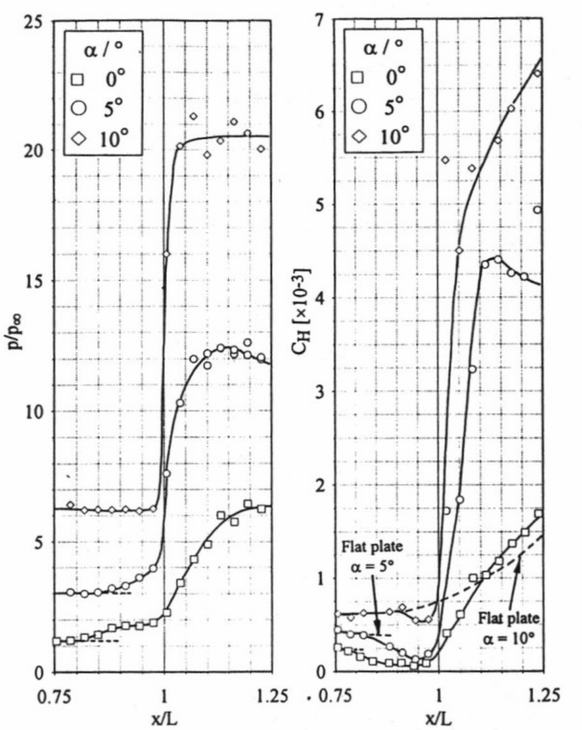


FIG. 12 THE EFFECT OF INCIDENCE ON THE PRESSURE AND HEAT TRANSFER DISTRIBUTIONS IN THE FLAP INTERACTION REGION FOR SEPARATED FLOWS [$M_\infty = 8.2$, $Re_\infty/cm = 9.0 \times 10^4$, $\beta = 10°$, sharp leading edge]

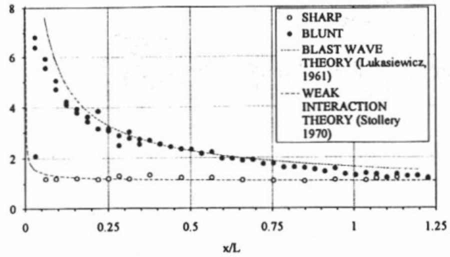


(a) pressure distribution

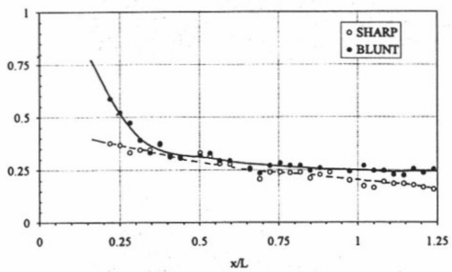


(b) heat transfer distribution

FIG. 13 THE EFFECT OF LEADING EDGE BLUNTNESS OF FLAT PLATE PRESSURE AND HEAT TRANSFER LEVELS

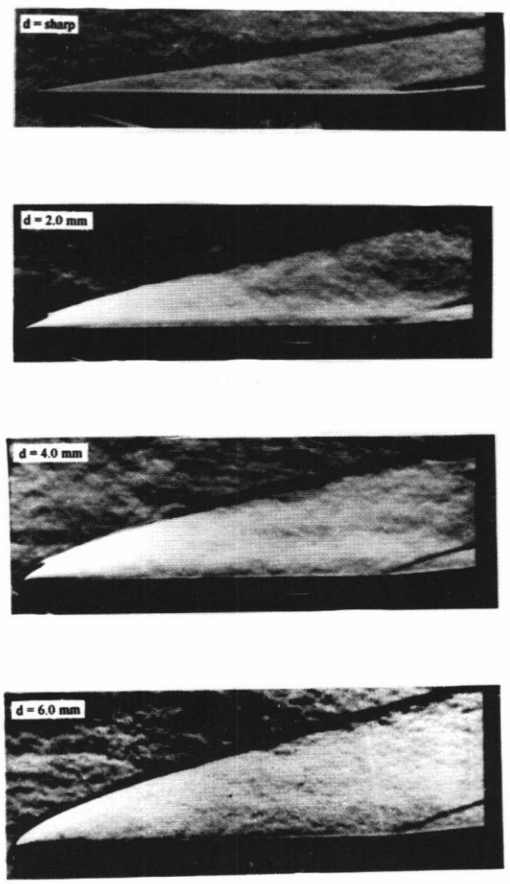


FIG. 14 THE EFFECT OF BLUNTNESS ON ATTACHED FLOWS [$M_\infty = 8.2$, $Re_\infty/cm = 9.0 \times 10^4$, $\alpha = 0°$, $\beta = 5°$, hemi-cylindrical LE]

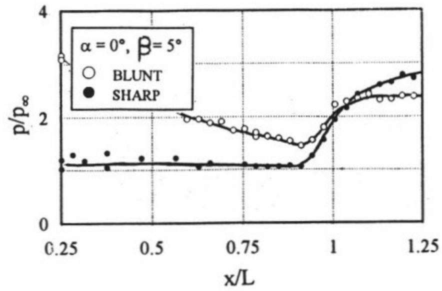


(i) pressure distribution

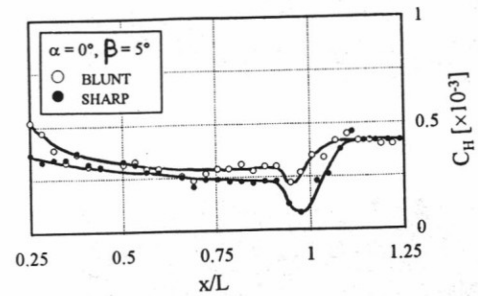


(ii) heat transfer distribution

FIG. 15(A) : THE EFFECT OF LEADING EDGE BLUNTNESS ON FLAP PRESSURE AND HEAT TRANSFER DISTRIBUTION
($M_\infty = 8.2$, $Re_\infty/cm = 9.0 \times 10^4$, $\alpha = 0°$, $\beta = 5°$)

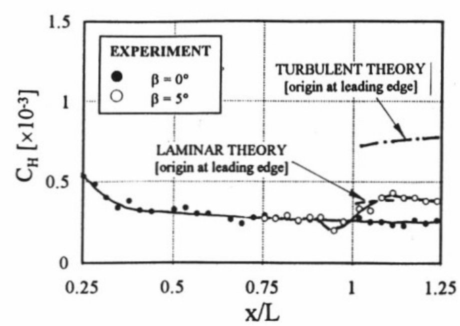


(i) blunt

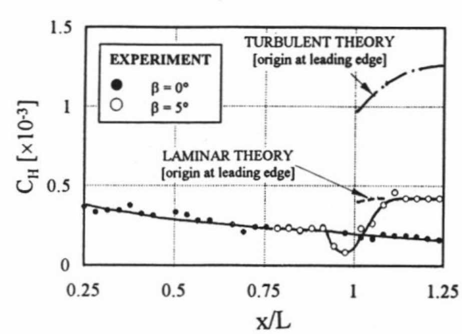


(ii) sharp

FIG. 15(B) : COMPARISON OF FLAP HEAT TRANSFER DISTRIBUTION WITH LAMINAR AND TURBULENT THEORY
($M_\infty = 8.2$, $Re_\infty/cm = 9.0 \times 10^4$, $\alpha = 0°$, $\beta = 5°$)

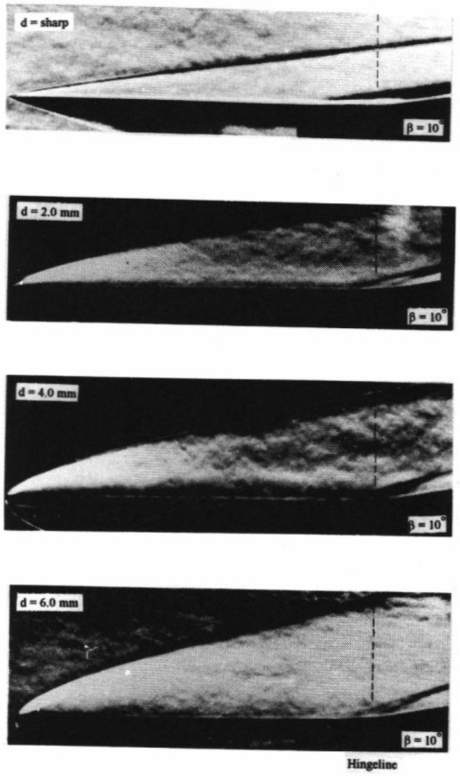


FIG. 16 THE EFFECT OF BLUNTNESS ON BOUNDARY LAYER SEPARATION [$M_\infty = 8.2$, $Re_\infty/cm = 9.0 \times 10^4$, $\alpha = 0°$, $\beta = 10°$, hemi-cylindrical LE]

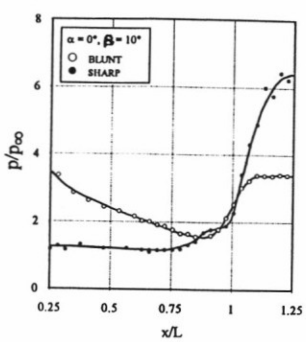


(i) pressure distribution

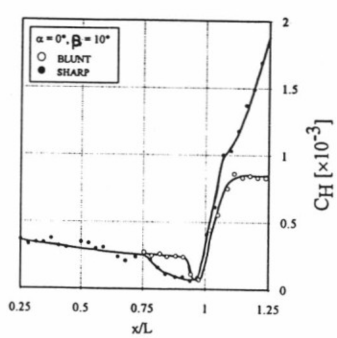


(ii) heat transfer distribution

FIG. 17(A) : THE EFFECT OF LEADING EDGE BLUNTNESS ON FLAP PRESSURE AND HEAT TRANSFER DISTRIBUTION
($M_\infty = 8.2$, $Re_\infty/cm = 9.0 \times 10^4$, $\alpha = 0°$, $\beta = 10°$)

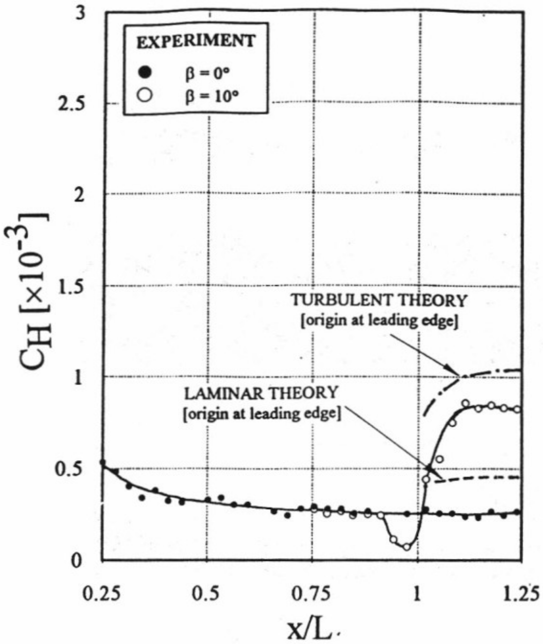


(i) blunt

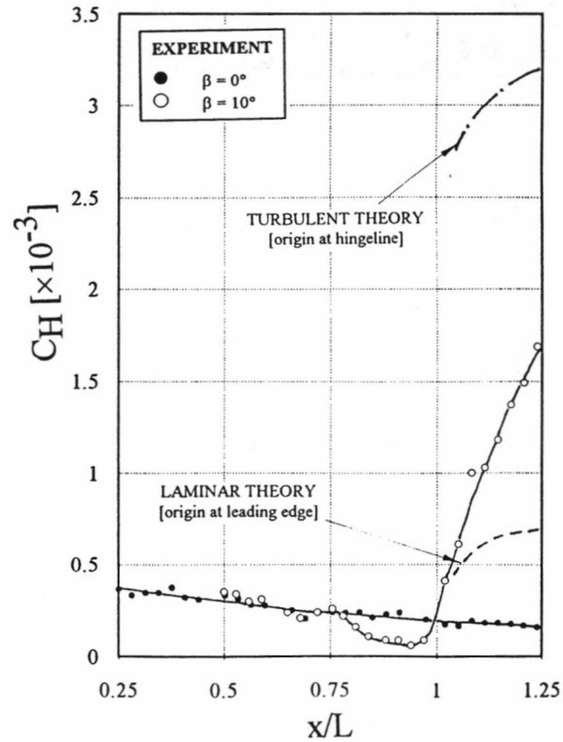


(ii) sharp

FIG. 17(B) : COMPARISON OF FLAP HEAT TRANSFER DISTRIBUTION WITH LAMINAR AND TURBULENT THEORY
($M_\infty = 8.2$, $Re_\infty/cm = 9.0 \times 10^4$, $\alpha = 0°$, $\beta = 10°$)

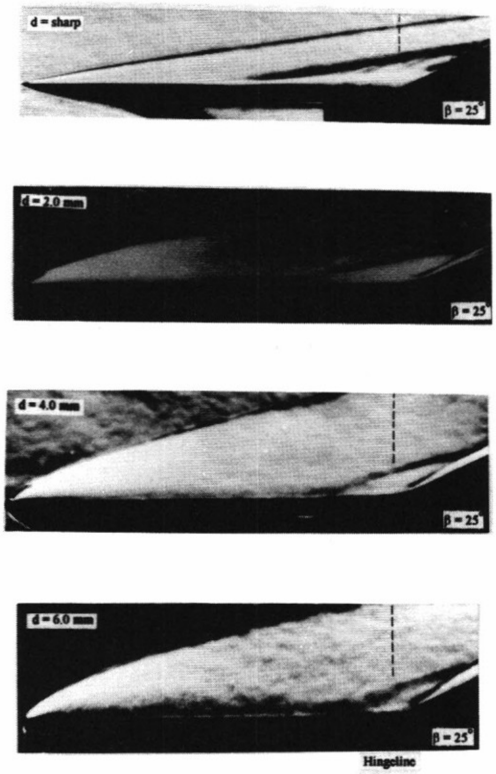


FIG. 18 THE EFFECT OF BLUNTNESS ON WELL-SEPARATED FLOWS
[$M_\infty$ = 8.2, $Re_\infty$/cm = 9.0 × $10^4$, α = 0°, β = 25°, hemi-cylindrical LE]

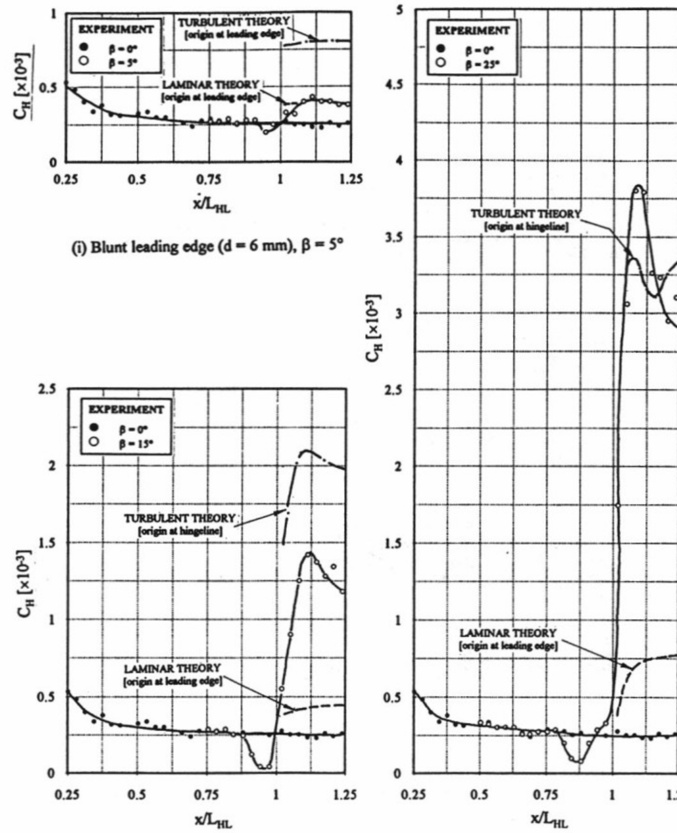


(ii) Blunt leading edge (d = 6 mm), β = 15°

(iii) Blunt leading edge (d = 6 mm), β = 25°

FIG. 20 COMPARISON OF THE FLAP HEAT TRANSFER DISTRIBUTIONS WITH PREDICTIONS FOR LAMINAR AND TURBULENT BOUNDARY LAYERS
[$M_\infty$ = 8.2, $Re_\infty$/cm = 9.0 ×$10^4$, α = 0°, d = 6.0 mm]

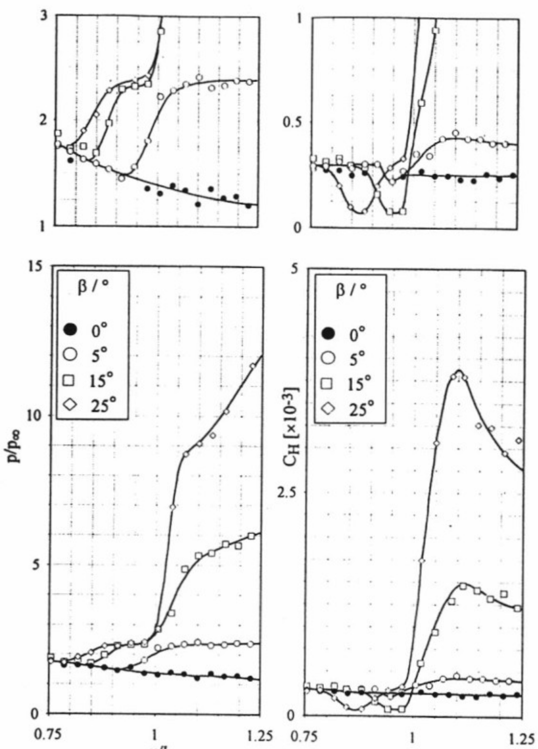


FIG. 19 THE EFFECT OF FLAP DEFLECTION ON THE PRESSURE AND HEAT TRANSFER DISTRIBUTIONS IN THE FLAP INTERACTION REGION FOR BLUNTNESS DOMINATED FLOWS [$M_\infty$ = 8.2, $Re_\infty$/cm = 9.0 ×$10^4$, d = 6.0 mm]

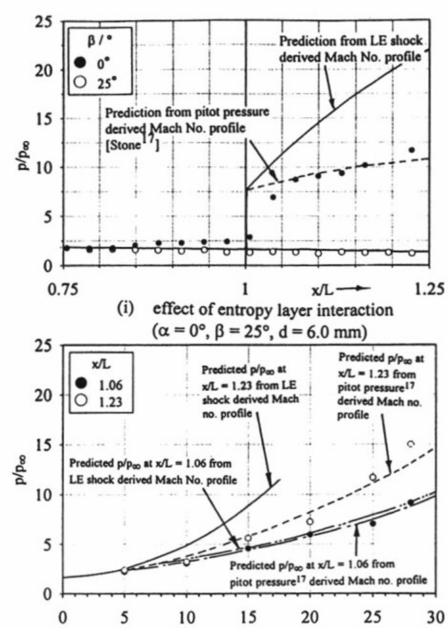


(ii) effect of flap deflection on entropy layer interaction
(α = 0°, d = 6.0 mm)

FIG. 21 THE EFFECT OF THE INTERACTION OF THE ENTROPY LAYER MACH SHEAR WITH THE FLAP SHOCK ON FLAP PRESSURE DISTRIBUTION [$M_\infty$ = 8.2, $Re_\infty$/cm = 9.0 ×$10^4$, α = 0°, d = 6.0 mm]